

Sub-micrometer aerosol particles in the upper troposphere/lowermost stratosphere as measured by CARIBIC and modeled using the MIT-CAM3 global climate model

Annica M. L. Ekman,^{1,2} Markus Hermann,³ Peter Groß,³ Jost Heintzenberg,³ Dongchul Kim,^{4,5,6} and Chien Wang⁴

Received 25 August 2011; revised 17 April 2012; accepted 17 April 2012; published 2 June 2012.

[1] In this study, we compare modeled (MIT-CAM3) and observed (CARIBIC) sub-micrometer nucleation (N_{4-12} , $4 \leq d \leq 12$ nm) and Aitken mode (N_{12} , $d > 12$ nm) particle number concentrations in the upper troposphere and lowermost stratosphere (UT/LMS). Modeled and observed global median N_{4-12} and N_{12} agree fairly well (within a factor of two) indicating that the relatively simplified binary H_2SO_4 - H_2O nucleation parameterization applied in the model produces reasonable results in the UT/LMS. However, a comparison of the spatiotemporal distribution of sub-micrometer particles displays a number of discrepancies between MIT-CAM3 and CARIBIC data: N_{4-12} is underestimated by the model in the tropics and overestimated in the extra-tropics. N_{12} is in general overestimated by the model, in particular in the tropics and during summer months. The modeled seasonal variability of N_{4-12} is in poor agreement with CARIBIC data whereas it agrees rather well for N_{12} . Modeled particle frequency distributions are in general narrower than the observed ones. The model biases indicate an insufficient diffusive mixing in MIT-CAM3 and a too large vertical transport of carbonaceous aerosols. The overestimated transport is most likely caused by the constant supersaturation threshold applied in the model for the activation of particles into cloud droplets. The annually constant SO_2 emissions in the model may also partly explain the poor representation of the N_{4-12} seasonal cycle. Comparing the MIT-CAM3 with CARIBIC data, it is also clear that care has to be taken regarding the representativeness of the measurement data and the time frequency of the model output.

Citation: Ekman, A. M. L., M. Hermann, P. Groß, J. Heintzenberg, D. Kim, and C. Wang (2012), Sub-micrometer aerosol particles in the upper troposphere/lowermost stratosphere as measured by CARIBIC and modeled using the MIT-CAM3 global climate model, *J. Geophys. Res.*, 117, D11202, doi:10.1029/2011JD016777.

1. Introduction

[2] Atmospheric aerosols affect climate directly through scattering and absorbing solar radiation [Charlson *et al.*, 1992] and indirectly through acting as cloud condensation nuclei, thereby altering the microphysical properties of clouds [Albrecht, 1989; Twomey, 1977]. Despite the recognized

importance of aerosols in cloud formation and for the radiative balance of the Earth, there are still large knowledge gaps regarding processes that shape the atmospheric aerosol population and its spatiotemporal distribution. This incomplete knowledge contributes to a large uncertainty regarding anthropogenic aerosol effects on clouds and climate and hampers our understanding of past and future climate sensitivity [Heintzenberg and Charlson, 2009; Lohmann and Feichter, 2005]. Clouds themselves are in turn important for the global aerosol distribution as aerosols can be removed, processed and formed within clouds. In contrast to the planetary boundary layer, only a few aerosol particle sources are relevant in the upper troposphere (UT) and lowermost stratosphere (LMS). However, these sources can still provide high numbers of new particles. Deep convective clouds are considered to be the most important contributor of new particle formation in the UT/LMS region [Hermann *et al.*, 2008]. Besides the generally low temperatures in the UT/LMS region, the high actinic flux in the vicinity of the clouds, the low condensational sink in the outflow region and the

¹Department of Meteorology, Stockholm University, Stockholm, Sweden.

²Bert Bolin Centre for Climate Research, Stockholm University, Stockholm, Sweden.

³Leibniz Institute for Tropospheric Research, Leipzig, Germany.

⁴Department of Earth, Atmospheric and Planetary Sciences, Massachusetts Institute of Technology, Cambridge, Massachusetts, USA.

⁵Universities Space Research Association, Columbia, Maryland, USA.

⁶NASA Goddard Space Flight Center, Greenbelt, Maryland, USA.

Corresponding author: A. M. L. Ekman, Department of Meteorology, Stockholm University, SE-10691 Stockholm, Sweden. (annica@misu.su.se)

Copyright 2012 by the American Geophysical Union.
0148-0227/12/2011JD016777

Table 1. Parameters for the CAM3 Aerosol Model^a

Aerosol Mode	Geometric Diameter Size Interval (nm)	Geometric Standard Deviation	Density (g cm ⁻³)	Hygroscopicity
BC	-	2.0	1.0	Hydrophobic
OC	-	2.0	2.0	Hydrophilic
NUC	0 < d < 5.84	1.59	1.8	Hygroscopic
AIT	5.84 < d < 31	1.59	1.8	Hygroscopic
ACC	>31	2.0	1.8	Hygroscopic
MBS	-	2.0	-	Hydrophilic
MOS	-	2.0	-	Hydrophilic

^aThe density of the MBS and MOS modes are volume ratio dependent. Standard deviations are based on the work by *Wilson et al.* [2001].

relatively high H₂SO₄ concentrations seems to support particle nucleation in connection with deep convection [*Clarke and Kapustin, 2002; Ekman et al., 2006; Hermann et al., 2003; de Reus et al., 1999; Ström et al., 1999; Twohy et al., 2002; Weigelt et al., 2009; Weigel et al., 2011*]. *Lee et al.* [2003, 2004] and *Zahn et al.* [2000] also suggested that upper tropospheric tropical cirrus clouds and mixing between tropospheric and stratospheric air more generally could trigger new particle formation events.

[3] Although the abundance of particulate mass is much lower in the free troposphere compared to the atmospheric boundary layer, the UT/LMS aerosol may still significantly impact on the radiative balance of the earth. Aerosol particles in this region may serve as surfaces for heterogeneous chemistry [*Bell et al., 2005; Borrmann et al., 1997; Søvdé et al., 2007*] and influence the formation of ice clouds [*Kärcher, 2003; Krämer et al., 2009*] and thereby indirectly impact on the radiative fluxes. The UT/LMS region also represents a source of the stratospheric aerosol [*Brock et al., 1995*] which is of relevance for stratospheric ozone destruction [*Hofmann and Solomon, 1989*]. The lack of representative in situ aerosol data for the UT/LMS was one of the reasons to initiate the CARIBIC project (Civil Aircraft for Regular Investigation of the Atmosphere Based on an Instrument Container, www.caribic-atmospheric.com). In this project, regular measurements of trace gases and aerosol particles have been conducted using a commercial aircraft platform first of Lufttransportunternehmen (LTU) International Airways and currently from Lufthansa [*Brenninkmeijer et al., 1999, 2007*]. Since November 1997 until today, two to four inter-continental measurement flights per month have been carried out on seven different flight routes. The respective data set (≈2000 flight hours) comprises more than 10 million particle concentration measurement points mainly in the northern hemispheric UT/LMS region.

[4] In the present study, we compare large-scale distributions of sub-micrometer aerosol concentrations obtained from CARIBIC with results from global model simulations using the MIT-CAM3 model [*Kim et al., 2008*]. MIT-CAM3 is a global climate model with a two-moment interactive aerosol physics and chemistry module involving seven different aerosol compounds and mixtures, namely three pure sulfate modes, one pure organic carbon (OC), one pure black carbon (BC), one sulfate/BC mixture (MBS; with BC core coated by sulfate shell) and one sulfate/OC mixture (MOS; a uniform mixture of OC and sulfate). The overall aim of the comparison is to learn more about the processes governing

the formation as well as spatial and temporal distribution of the UT/LMS sub-micrometer aerosol. As a first step toward this goal, we will evaluate the performance of MIT-CAM3 in terms of representing the spatiotemporal variability of the UT/LMS sub-micrometer aerosol particle number concentration. By examining MIT-CAM3 model biases, we may obtain a first indication on processes crucial for determining the UT/LMS sub-micrometer aerosol particle distribution. We may also identify difficulties that arise when comparing global model output with CARIBIC data. This may give us directions for future model sensitivity studies and point toward additional measurement data that are needed.

[5] The paper is organized as follows: In section 2 we give an overview of the MIT-CAM3 model and the CARIBIC data set and describe the data processing necessary in order to make the comparison. In section 3, results from approximately nine years of CARIBIC measurements and five years of model simulations using three different versions of the MIT-CAM3 model are presented and compared. A discussion and conclusions are found in section 4.

2. Method

2.1. MIT-CAM3

[6] The meteorological part of the MIT-CAM3 model is the NCAR Community Atmospheric Model version 3 [*Collins et al., 2006*]. Coupled to this model is a multimode two-moment aerosol model of sulfate and carbonaceous compounds [*Kim et al., 2008*]. The aerosol module is based on the work by *Wilson et al.* [2001] and has been developed to include seven aerosol modes defined by particle size and hygroscopicity (Table 1). The model is designed to predict mass and number concentrations of three pure sulfate modes; the nucleation (NUC), Aitken (AIT) and accumulation (ACC) mode, one pure organic carbon mode (OC), one pure black carbon mode (BC), one BC/sulfate mixed mode (MBS: a BC core with sulfate shell mixture) and one OC/sulfate mixed mode (MOS; a uniform mixture). The particle size distribution for each aerosol mode is obtained by assuming a lognormal distribution and using a prescribed standard deviation for each mode (Table 1). Below follows a brief summary of the MIT-CAM3 model characteristics. For a more comprehensive description, cf. *Kim et al.* [2008].

[7] New particles are formed in the model through binary H₂SO₄-H₂O nucleation [*Vehkamäki et al., 2002*], which for the UT/LMS region should be suited to explain observations [*Clement et al., 2002; English et al., 2011*], in particular as the particle number a few hours after nucleation seems to be insensitive to the exact nucleation mechanism [*Clement et al., 2006; English et al., 2011*].

[8] In the model, the particles can grow through coagulation (intra and inter-mode for pure sulfate particles and the mixed modes) and condensation of H₂SO₄ on the particles. Gas-phase SO₂ oxidation provides the primary source of H₂SO₄ where the H₂SO₄ concentration is predicted by an interactive sulfur module [*Barth et al., 2000*]. Pure BC and OC particles are assumed to age into the MBS and MOS modes through a constant aging time of 40 and 20 h, respectively. In addition to the prescribed aging time, the aging process is also limited by the amount of condensable H₂SO₄. Note that in the model, all SOA is emitted at the surface, i.e., there is no condensation of organic vapors in

the atmosphere to form secondary organic particles. The MIT-CAM3 model has been evaluated versus observations of the various aerosol compounds in *Kim et al.* [2008]. In the UT, the model was found to be in good agreement, or slightly overestimate, the mass concentration of sulfate compared to measurements performed during different aircraft campaigns (ACE-Asia, PEM-West A, PEM-West B and PEM-Tropics A [*Kim et al.*, 2008, Figures 12 and 13, and references therein]).

[9] All aerosols undergo transport, sedimentation, dry deposition and impaction scavenging by precipitation in the model, with different scavenging efficiencies and dry deposition rates for each aerosol mode and for different hydrometeor types. The impaction-scavenging rate is governed by an experimentally based efficiency factor which is equal to 30 (NUC), 6 (AIT), 3.5 (BC, OC, MBS, MOS) and 1 (ACC). The hygroscopic and hydrophilic particles in the model can also serve as cloud condensation nuclei (CCN) where the activated number of CCN at each time step is calculated using the κ -Köhler assumption [*Petters and Kreidenweis*, 2007]. To simplify the calculations, and similar to [*Adams and Seinfeld*, 2002], a prescribed supersaturation at cloud base of 0.1% for OC and 0.2% for sulfate and mixed aerosols is used and all particles in-between 500 and 2000 m altitude may be nucleation scavenged.

[10] Emissions of BC, SO₂ and primary OC are taken from the 1° × 1° emission inventory by the MIT Emission Prediction and Policy Analysis Model (EPPA) [*Babiker et al.*, 2001; *Mayer et al.*, 2000; *Wang*, 2004] for the year 1990, and are constant throughout the whole model year. It should be noted that whereas the SO₂ emission database is for the year 1990, the CARIBIC observations are conducted during 1997–2009. During this period, SO₂ emissions have generally increased over Asia and decreased over Europe and North America [*Gislason and Torssander*, 2006; *Lu et al.*, 2010; *Vestrenge et al.*, 2007].

[11] Besides SO₂ emissions, the model also includes emissions of dimethylsulfide (DMS) provided by CAM3 (and based on *Kettle et al.* [1999]). Note that the DMS can be oxidized to SO₂ and hence also contribute to new particle formation. In addition to primary OC, the production of secondary organic aerosols (SOA) are calculated using biogenic VOCs emissions (isoprene and monoterpene) based on a yield coefficient suggested by *Griffin et al.* [1999]. Both DMS and VOC emissions have a monthly variation.

[12] The time step for advection and physics is 30 min in the model. A 26-layer hybrid vertical coordinate is applied, i.e., sigma coordinates near the surface and pressure levels in the UT/LMS region. The horizontal resolution is 2.5° in the longitudinal and 2° in latitudinal direction. An observed 20-year monthly mean sea surface temperature is used as an ocean boundary.

[13] Two different versions of the MIT-CAM3 model are utilized in the present study, one where the aerosol cycle is modeled as described in the section above (*EEA*) and one where no aerosol mixtures are allowed in the model, i.e., the MOS and MBS modes are absent (*EEE*), cf. also the description in *Kim et al.* [2008]. Five years of model data are used for the analysis of the *EEA* and *EEE* simulations and as a default, monthly averages are used as model output. The procedure of monthly averaging may create a bias in the data as the monthly average may differ substantially from a monthly median value based on instantaneous output. We therefore in addition

conduct a 1-year simulation with 6-h instantaneous output frequency for the *EEE* simulation (*EEE-instant*). Note that the CARIBIC data is processed in the same manner for all comparisons with all versions of the MIT-CAM3 model (as described in the next section).

[14] For comparison with the CARIBIC data, the model output are gridded into 15° × 15° grid cells along the CARIBIC flight tracks and data from model levels 14 to 16 (approximately 200 to 300 hPa) are used to cover the typical aircraft cruise altitudes [cf. *Heintzenberg et al.*, 2011]. The modeled aerosol size distribution is re-calculated and redistributed to the aerosol size bins of CARIBIC (cf. Section 2.2). For statistical reasons, we do not separate between tropospheric and stratospheric air masses (A distinction between tropospheric and stratospheric air based on in situ ozone measurements and a chemical tropopause definition is available from CARIBIC [cf. *Zahn and Brenninkmeijer*, 2003]). When using model data from level 14 to 16, we obtain a slightly lower fraction of stratospheric versus tropospheric air in the extra-tropics compared to CARIBIC measurements (approx. 10% lower fraction in the subtropics and 30% lower at midlatitudes). If we instead analyze model data from levels 13 to 15 (not shown here), the fraction of stratospheric air agrees better with observations (less than 10% difference), but the agreement in terms of model pressure instead becomes worse. More importantly, the overall results and conclusions of the study do not change significantly if we use somewhat different model levels, i.e., 13–15 or 15–17 instead of 14–16.

2.2. CARIBIC Data Processing

[15] The CARIBIC aerosol data used in this study were measured during the period of November 1997 to October 2009, with a break for aircraft changeover from LTU to Lufthansa from May 2002 to December 2004 (www.caribic-atmospheric.com). Altogether, data from 208 inter-continental flights (~2000 flight hours) are available, covering a large fraction of the northern midlatitudes (Figure 1). About 92% of these measurements were carried out between 8.5 and 12.0 km altitude [cf. *Heintzenberg et al.*, 2011, Figure 1]. In CARIBIC, integral particle number concentrations are measured for particles larger than 4, 12 and 18 nm, respectively, using Condensation Particle Counters (CPCs) [*Hermann and Wiedensohler*, 2001]. While the number concentration of particles larger than 12 nm can be considered as the Aitken mode particle number concentration (N_{12}) (the contribution of the accumulation mode in the UT/LMS is generally small), the difference between the readings of the first two particle counters (N_{4-12}) can be considered as the nucleation mode particle number concentration. CARIBIC aerosol data can thus be used to identify regions and frequency of new particle formation in the UT/LMS, but without any additional information on precursor gas concentrations (e.g., H₂SO₄) the data cannot be used to discriminate between different particle formation mechanisms. All measured particle number concentrations were corrected for particle losses in the inlet and in the sampling line in a similar way as described in *Hermann et al.* [2001]. Thus, all particle losses in the diffuser of the new inlet (Lufthansa Airbus) had to be assumed to be the same as determined in the wind tunnel experiment for the old inlet.

[16] Furthermore raw concentrations were corrected for pressure-dependent CPC flow rates, for CPC counting

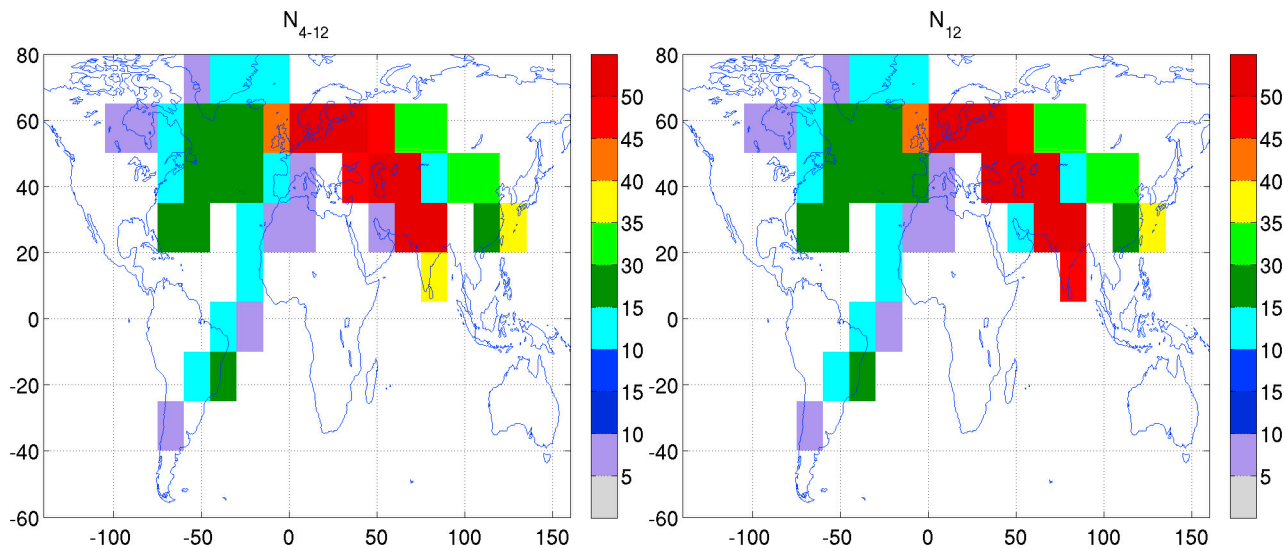


Figure 1. Total number of flights per $15^\circ \times 15^\circ$ grid cell for CARIBIC measurements of (left) N_{4-12} and (right) N_{12} between Nov. 1997 and Oct. 2009. Note that the figure only includes grid cells fulfilling the criteria of having at least five flights per grid cell and at least one flight during winter and summer.

efficiencies, and for coincidence in the CPC optics [Hermann, 2000]. Finally, the data were transferred to STP conditions (1013.25 hPa, 273.15 K). During sampling, the measured particles experience a strong heating from -60°C to -30°C outside the aircraft to about $+30^\circ\text{C}$ in the measurement container. Consequently, the measured particles lose the major part of their water and can be considered to be almost dry (and are thus also compared to the modeled dry particle distribution). Moreover, volatile particle material can partly evaporate due to this strong heating, while sulfuric acid is assumed to remain on the particles [cf. Hermann *et al.*, 2001].

[17] Comparing the CARIBIC data to the output of a global atmospheric model requires some statistical considerations. Independent of the absolute number of data points obtained during a CARIBIC flight, each flight represents only one meteorological situation over a certain region of the globe. Consequently the number of flights per grid cell (Figure 1) is equally important with respect to representativeness as the absolute number of data points. In this study, as a subjective compromise, at least five flights, and thereof at least one flight in each of the two seasons summer and winter were set as minimum requirement for the analysis of annual median aerosol concentrations. For the seasonal analysis, the requirement was at least two flights per grid cell to yield a valid cell for comparison. In this study, two expanded seasons were used to improve the statistics, northern hemispheric summer (May through September) and northern hemispheric winter (November through March). For the comparison, only CARIBIC data between 200 and 300 hPa were used.

3. Results

3.1. Nucleation Mode Particle Number Concentration ($4 \leq d \leq 12$ nm)

3.1.1. Global Annual Median Concentration

[18] Figure 2a displays the annual median N_{4-12} number concentration as observed by CARIBIC. The median concentration is generally low (below 1000 cm^{-3} ; cf. Table 2).

Higher concentrations (up to 1500 cm^{-3}) are generally found close to regions with high emissions of SO_2 and primary particles as well as over regions with frequent deep convection, i.e., over Southeast Asia, Europe, West Africa and along the East coast of North America. The modeled global median N_{4-12} number concentration agrees relatively well with observations (Table 2) with a slight underestimate for the *EEA* simulation (35% compared to the $2^\circ \times 2^\circ$ average), a slight overestimate for the *EEE* simulation (18%) and a good agreement (less than 2% difference) for the *EEE-instant* simulation. However, the geographical distribution is not captured as well by the model (Figures 2 and 3a). For all simulations, the correlation of the median aerosol concentration with the observations (correlating the median value of the CARIBIC observations in each grid cell with the median value of MIT-CAM3) is very poor (correlation coefficient close to zero). In tropical regions, N_{4-12} is underestimated (by up to 70%), whereas the concentrations are overestimated (up to several orders of magnitude) at higher latitudes (Figure 3a). The overestimate is most pronounced over large parts of central Asia and the Arctic region, particularly in the *EEE* and *EEE-instant* simulations (Figure 2). The underestimate may be caused by either a too low production of new particles in the model or by a too fast growth of the particles into the Aitken mode. The overestimate can either be caused by a too long residence time of the N_{4-12} particles (i.e., too slow growth or too little vertical transport/mixing or scavenging by hydrometeors) or too high production rate.

3.1.2. Number Frequency Distributions and Vertical Profiles

[19] A number frequency distribution for the CARIBIC observation data points averaged over $2^\circ \times 2^\circ$ grid cells (i.e., approximately the same resolution as the MIT-CAM model data) for the tropics and midlatitudes (Figures 4a and 5a, respectively) reveals an approximately lognormal distribution for the CARIBIC particle data, in agreement with results from previous research campaigns [Thompson *et al.*, 1999; Heintzenberg *et al.*, 2011] and theoretical considerations

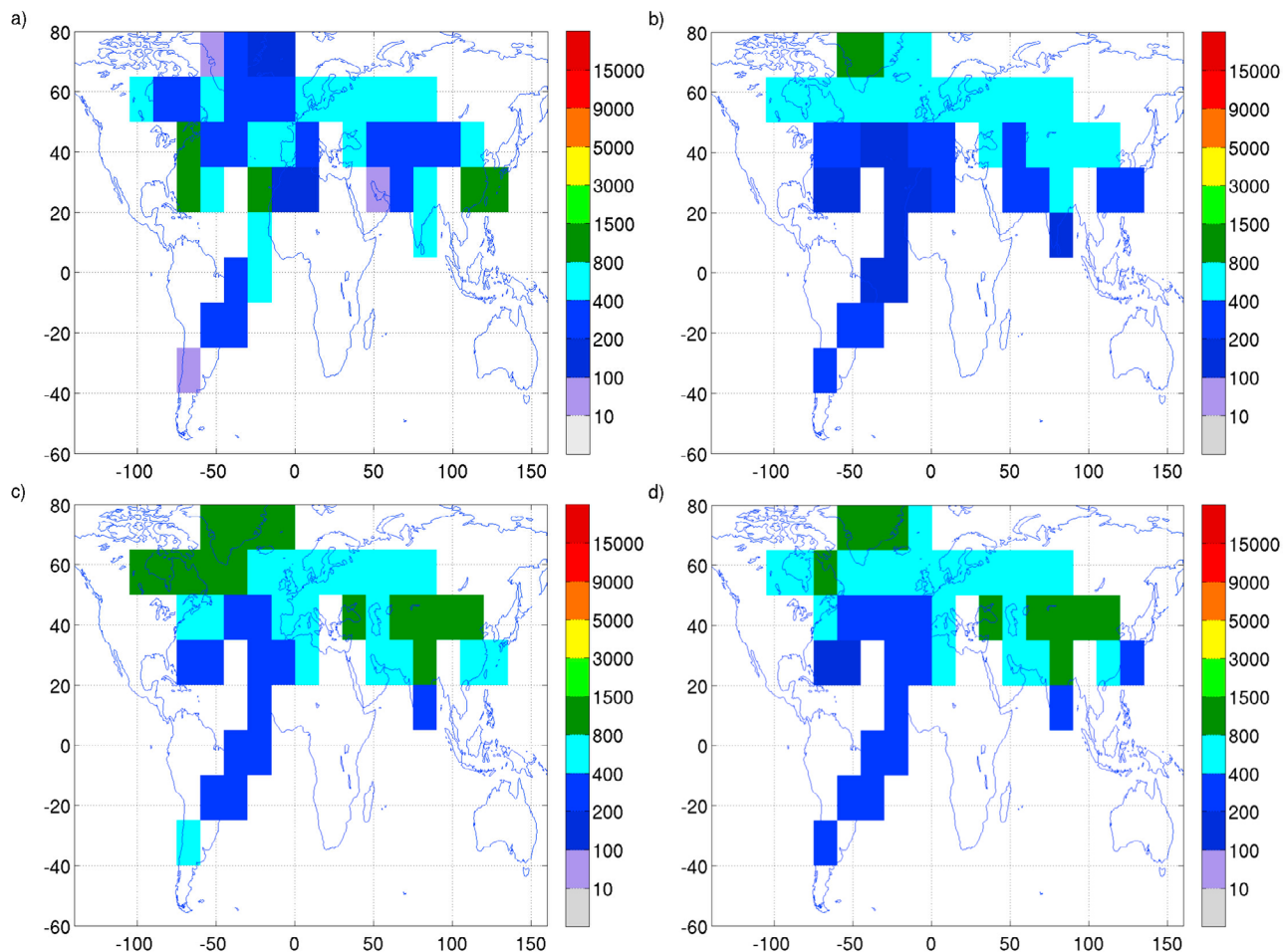


Figure 2. Annual median N_{4-12} number concentration (particles cm^{-3} at STP) between 200 and 300 hPa for (a) CARIBIC observations, (b) *EEA* simulation, (c) *EEE* simulation and (d) *EEE-instant* simulation. Note that the color scale is chosen for an easy comparison with *Heintzenberg et al.* [2011].

[*Ott*, 1990]. The lognormal shape indicates that the aerosol particle frequency distribution is a result of successive, random dilution events associated with atmospheric turbulence on a variety of scales. For the N_{4-12} particles, which are normally rather short-lived, it is also possible that a varying source strength contributes to the shape of the distribution. Comparing the model results with the CARIBIC data (Figures 4 and 5), it is evident that the model displays a much narrower frequency distribution compared to the observations, especially in the *EEA* and *EEE* simulations. Both the *EEA* and the *EEE* simulations also display skewed lognormal distributions, a result which is different compared to the observations. This result points toward a too small vertical and/or horizontal diffusive mixing in the model. A less variable source may also contribute to the discrepancy. It is interesting to note the difference in frequency distributions between the *EEE* simulation and the corresponding simulation with instantaneous output, i.e., the *EEE-instant* simulation. In the model, the concentration of N_{4-12} particles is generally low in the boundary layer [cf., e.g., *Kim et al.*, 2008, Figure 6], supporting the assumption of in situ UT/LMS particle production. The *EEE-instant* simulation (Figures 4d and 5d) suggests a more bi-modal structure in the frequency distribution compared to the other simulations,

especially in the tropics. The bi-modal structure indicates that the sampling occurs in two significantly different air masses, i.e., that there may be a diurnal variation in N_{4-12} in the model. This is a reasonable result if we assume that most of

Table 2. Global Median and Mean Particle Number Concentrations Between 200 and 300 hPa for CARIBIC Data and MIT-CAM3 Simulations^a

	CARIBIC				
	CARIBIC ($2^\circ \times 2^\circ$ Average)	EEA	EEE	EEE-Instant	
	$N_{4-12} (\times 10^2)$				
Global median	4.4	5.5	3.6	6.5	5.4
Global mean	17.9	16.1	4.3	13.0	10.0
Summer median	5.1	5.5	4.2	9.0	7.1
Winter median	4.8	4.9	3.4	5.2	4.6
	$N_{12} (\times 10^3)$				
Global median	2.5	2.7	4.4	4.7	4.7
Global mean	4.3	4.2	4.7	5.3	5.1
Summer median	3.4	3.1	5.4	6.1	5.7
Winter median	2.0	2.2	3.1	3.3	3.3

^aAlso displayed are NH summer (May–September) and winter (November–March) median concentrations. CARIBIC data are shown both as original data and median and mean of $2^\circ \times 2^\circ$ averages. All number concentrations are given in particles cm^{-3} STP.

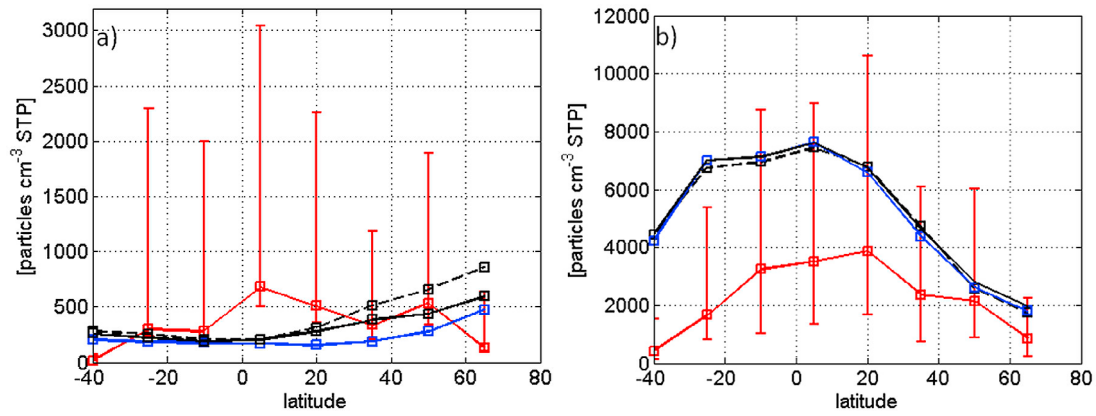


Figure 3. Latitudinal median (a) N_{4-12} and (b) N_{12} number concentration (particles cm^{-3} at STP) between 200 and 300 hPa for CARIBIC observations (red line), *EEA* simulation (blue line), *EEE* simulation (full black line) and *EEE-instant* simulation (black dashed line). Error bars denote 25- and 75-percentiles. Only data from grid cells displayed in Figure 1 are included in the comparison.

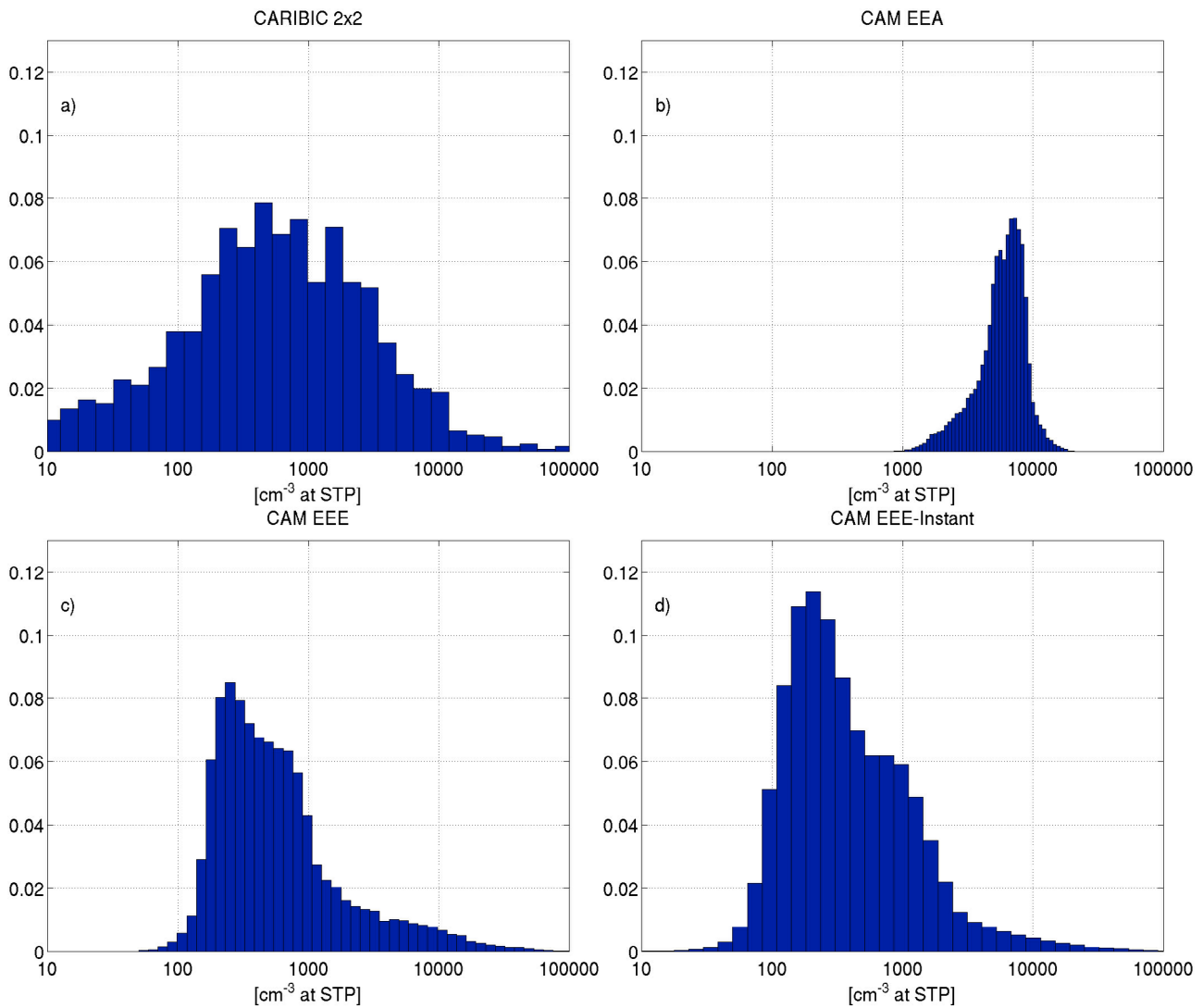


Figure 4. Frequency distribution for N_{4-12} particles in the tropics (25°S to 25°N) for all measurement/model data points in all the grid cells displayed in Figure 1.

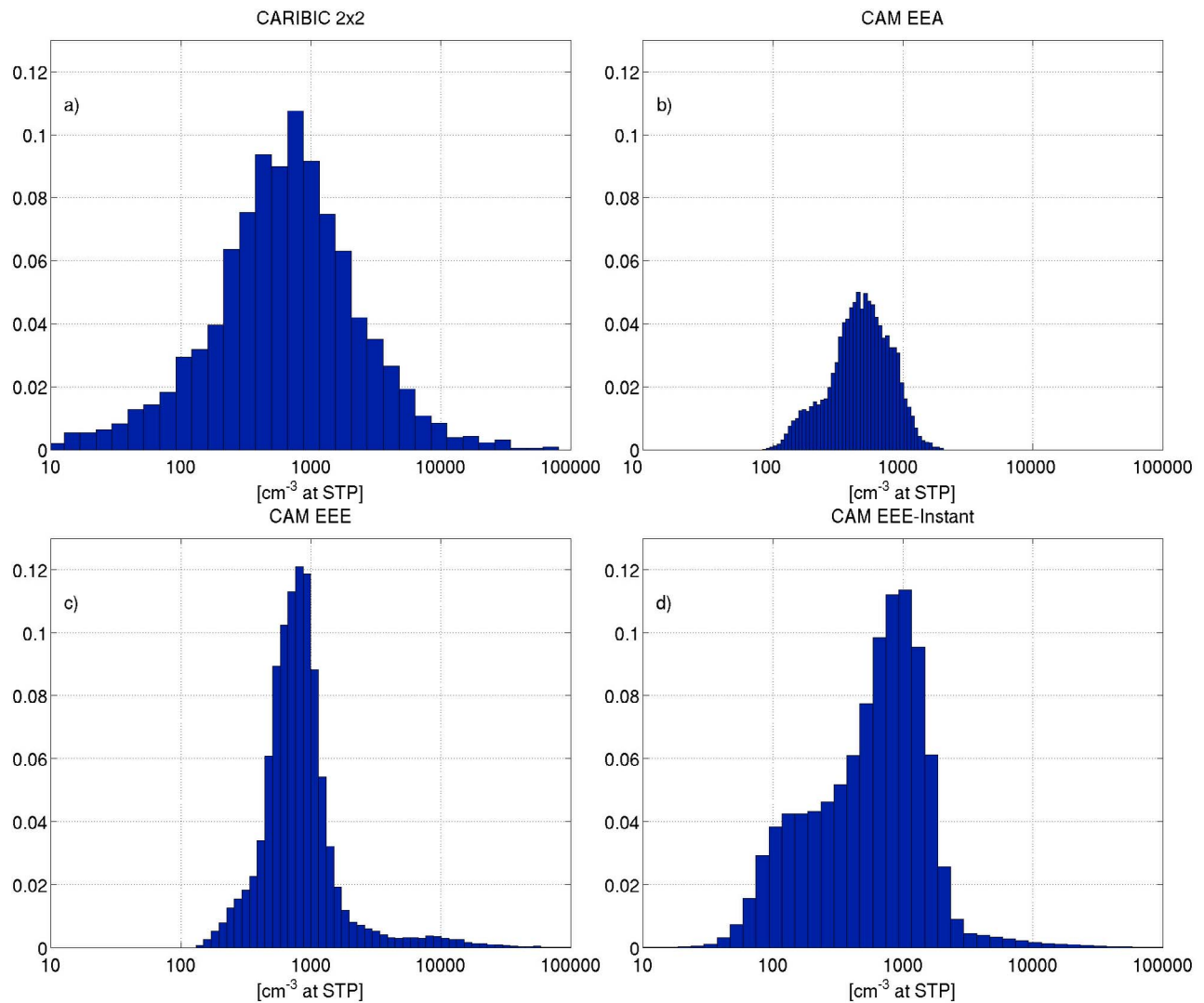


Figure 5. Frequency distribution for N_{4-12} particles at midlatitudes (35°N to 65°N) for all measurement/model data points in all the grid cells displayed in Figure 1.

the N_{4-12} particles are formed within deep convective outflows, as deep convective activity often has a diurnal cycle [Hendon and Woodberry, 1993]. Please note in this context that because of the fixed flight schedule of the CARIBIC aircraft, the CARIBIC aerosol measurements are partly biased toward certain local times of day, i.e., in some regions the measurements are always carried out at about the same local time of the day. This bias is strongest on the South-America route (cf. Figure 2 and discussion in Heintzenberg *et al.* [2011]) and may affect mainly the median concentrations of the short-living nucleation mode particles, which are closely related to cloud occurrence and photochemistry [Hermann *et al.*, 2003; Weigelt *et al.*, 2009]. Larger particles live much longer than a day and thus respective concentrations are less dependent on the local time of measurement.

[20] A vertical profile of potential temperature versus all tropical CARIBIC nucleation mode data (Figure 6) reveals that high concentrations ($>1 \times 10^3$) of newly formed particles may frequently be found in a broad altitude interval between 320 and 365 K (cf. 75 and 90 percentiles). There is a slight increase in N_{4-12} with altitude from 320 K up to

approximately 355 K. After that, there is a decrease with altitude to about 365 K. The occurrence of particle formation within this altitude range, with maximum median number concentrations around 355 K of approx. $7.5 \times 10^2 \text{ cm}^{-3}$ (corresponding to $1.6 \times 10^3 \text{ mg}^{-1}$) is in broad agreement with data presented by e.g., Wilson *et al.* [1991], Brock *et al.* [1995], Borrmann *et al.* [2010] and Weigelt *et al.* [2011] and indicates that new particles generated in deep convective outflows close to the tropopause are transported into the lower part of the tropical transition layer (TTL) and the LMS. Comparing with the model simulations, it is first of all noted that the atmosphere is colder in the model than in the CARIBIC data for this altitude range. The cold bias is a well-known feature in the CAM3 model version and is discussed further in, e.g., Boville *et al.* [2006]. We note that this cold bias may induce a too high nucleation rate in the model as the parameterization by Vehkamäki *et al.* [2002] is strongly dependent on temperature. However, due to the long time step of the model (30 min), and as verified using box model calculations (not shown), the most important process to determine the overall N_{4-12} concentration is

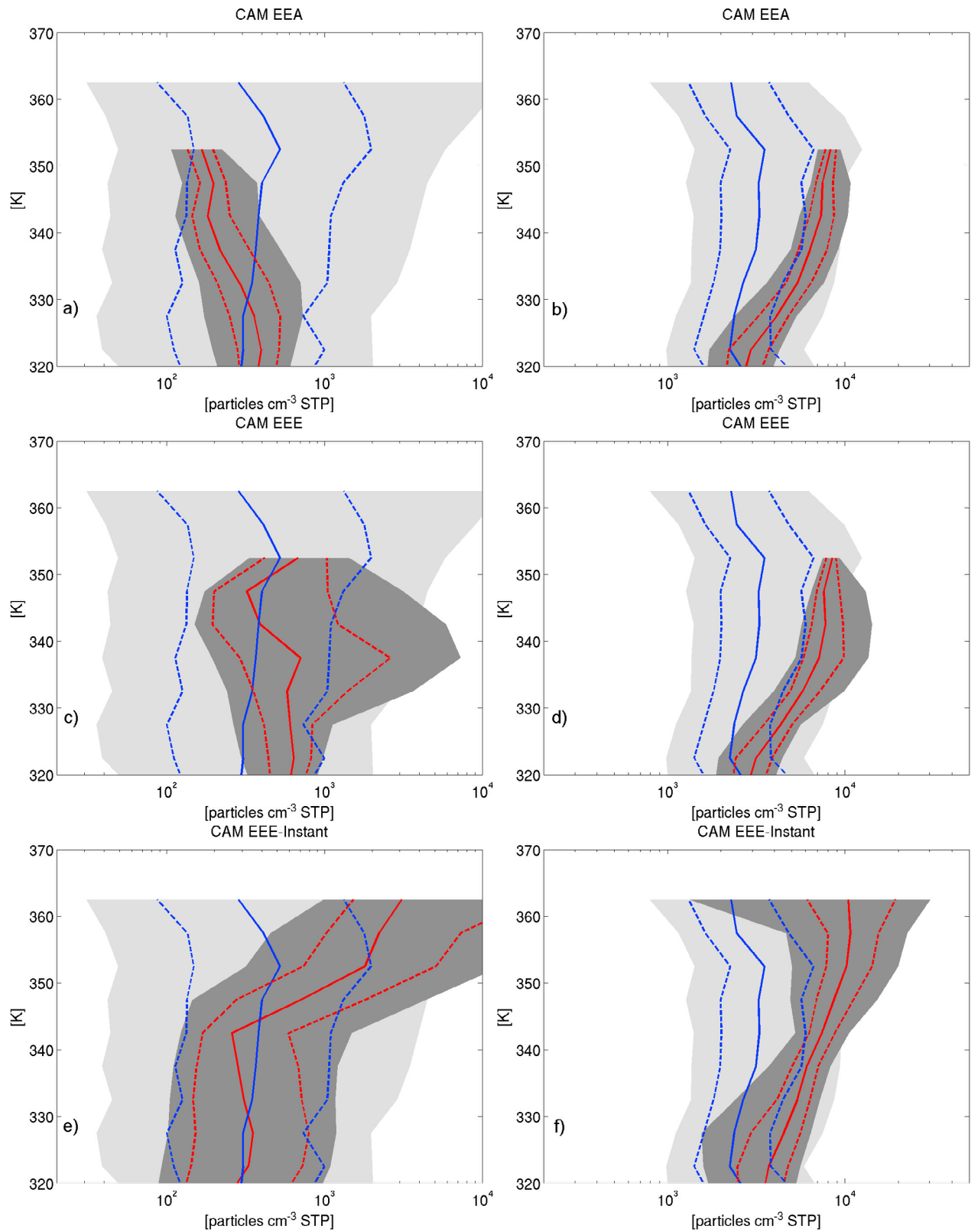


Figure 6. Vertical profiles of potential temperature versus (a, c, and e) N_{4-12} and (b, d, and f) N_{12} in the tropics (25°S to 25°N). CARIBIC data in blue full line (median), blue dashed lines (25 and 75 percentiles) and light gray shading (10 and 90 percentiles). CAM *EEA* (Figures 6a and 6b), CAM *EEE* (Figures 6c and 6d) and CAM *EEE-Instant* (Figures 6e and 6f) simulations in red full line (median), red dashed lines (25 and 75 percentiles) and dark gray shading (10 and 90 percentiles). Both CARIBIC and model data have been binned in 5 K intervals between 320 and 365 K.

coagulation and the exact value of the nucleation rate plays a secondary role [cf. also *English et al.*, 2011].

[21] Both the *EEA* and *EEE* simulations display in general much less variability in N_{4-12} than the CARIBIC data (Figures 6a, 6c and 6e, cf. e.g., 25 and 75 percentiles), whereas the *EEE-instant* simulation shows somewhat better agreement in this aspect. For the *EEA* simulation, the model displays no high ($>1 \times 10^3$) concentrations of N_{4-12} particles for the whole altitude range. In *EEE*, the simulated median N_{4-12} is in better agreement with observations than in *EEA*. In the UT/LMS region, simulated H_2SO_4 concentrations are substantially higher in *EEE* than in *EEA* (on average $\sim 40\%$, not shown). As the same amount of SO_2 is transported to the UT/LMS region in both model versions, this result indicates that a larger amount of H_2SO_4 condenses on pre-existing aerosols in *EEA* than in *EEE*. In other words, there must be a substantial vertical transport of mixed (MBS and MOS) aerosols in *EEA* and this transport may be overestimated by the model. The *EEE* simulation displays maximum median concentrations around 335 K which is at an approximately 20 K lower temperature than the observations. The *EEE-instant* simulation displays an increasing aerosol concentration with altitude above approximately 345 K. As the *EEE-instant* results are based on instantaneous output, this implies that there are a number of short-term events in the model where high concentrations of new particles are produced at high altitudes.

3.1.3. Seasonal Variability

[22] The average difference between the global median summer and winter N_{4-12} number concentration is small in the CARIBIC observations (Table 2), however for individual regions, mainly in the tropics, it is still substantial (more than a factor of two, cf. Figure 7). The *EEE* and *EEE-instant* simulations display a similar seasonal variability as the observations with higher values in summer, mainly over Southeast Asia. However, the seasonal variability is overestimated by the model, especially in the *EEE* simulation (Table 2). The *EEA* simulation displays a weak seasonal variability, similar to the CARIBIC observations (Table 2). Both summer and winter values are however underestimated by the *EEA* simulation (Figure 7 and Table 2).

[23] The annual cycle of the median aerosol concentration over three different study regions (displayed in Figure 8) are shown in Figure 9. The variability in the observations is large, and all model simulations generally display N_{4-12} concentrations within the 25–75% percentile range of the CARIBIC data. In the following discussion, all temporal variability is significant at a 95% confidence level (using a Student's *t* test) if nothing else is stated. For the U.S. region, there is a maximum in the N_{4-12} concentration in September in the CARIBIC data and two (non-significant) smaller maxima in February and June. None of the model versions display a similar annual cycle as the observations for this region. For the European region, the CARIBIC data displays a similar annual variability as for the U.S. region and here the maxima in February and September/October are both significant. The modeled annual cycle does not agree with the observations with the highest values noted in May (*EEE-instant* and *EEA* simulations) or August–September (*EEE* simulation). Over India, the CARIBIC observations display a maximum in June (significant at 90% level) and a smaller one in October–November (significant at 90% level). Two

weak maxima in the N_{4-12} concentration are also visible in the *EEA* simulation in May and October, which is in qualitative agreement with the observations. The *EEE* and *EEE-instant* simulations display a substantial maximum in July–August, which for the *EEE-instant* simulation is within the uncertainty range of the observations. The *EEE* simulation has a clear high bias in summer indicating that the monthly averaging of the model output may be an issue.

[24] It should be noted that in the present study, constant annual SO_2 (and primary particle) emission rates are applied in the MIT-CAM model. This may be one reason for the poor agreement between CARIBIC and modeled output data in terms of the annual cycle in N_{4-12} concentration. In addition, the division into N_{4-12} and N_{12} contains uncertainties, both for the model and for the observations. The lognormal modes defining the NUC and AIT mode in the model do not exactly correspond to the size bins of the CARIBIC data. The modeled particle size distribution must therefore be redistributed into the N_{4-12} and N_{12} bins based on an assumed standard deviation of the different model modes. For the CARIBIC data, the N_{4-12} concentration is calculated as the difference between the readings of the first two CPCs (cf. Section 2.2.1) and this may introduce large uncertainties if the N_{4-12} concentration is below about 200 particles cm^{-3} STP.

3.2. Aitken Mode Particle Number Concentration ($d > 12$ nm)

3.2.1. Global Annual Median Concentration

[25] For N_{12} , the CARIBIC observations display a maximum in the annual median N_{12} number concentration along the equator (where deep convective clouds are found frequently) and with the highest concentrations near strong SO_2 and primary particle sources, i.e., over Asia, Eastern U.S. and to some extent also over Europe (Figures 10 and 3b). All model simulations overestimate the median concentration (by 63–74%, cf. Table 2), but the geographical distribution agrees fairly well with observations (correlation coefficients between 0.68 and 0.71, cf. also Figure 3b). In general, the largest overestimate by the model appears to be located downwind the emission source regions and over South America. For this latter region the bias toward certain local measurement times in the CARIBIC data might partly explain at the discrepancy (cf. Section 3.1.2). Both the model simulations and the CARIBIC observations display similar latitudinal gradients in the northern hemisphere (Figure 3b), whereas the longitudinal gradients, for instance in the band 20–35°N, are not well captured by the model (Figure 10). This could be an indication of a too long residence time of the N_{12} particles in the model. In contrast to the geographical distribution of N_{4-12} , the three different model versions display a more coherent pattern. It should be noted from a chemical and aerosol microphysical perspective that the model may be expected to perform better in predicting N_{12} compared to N_{4-12} , as the former is less sensitive to variations in short-lived chemical compounds (such as SO_2 and OH), coagulation processes and the choice of new particle formation parameterization. The predicted N_{12} may on the other hand be more sensitive to dynamical processes such as stratospheric-tropospheric exchange (due to the longer residence time of N_{12} compared to N_{4-12}).

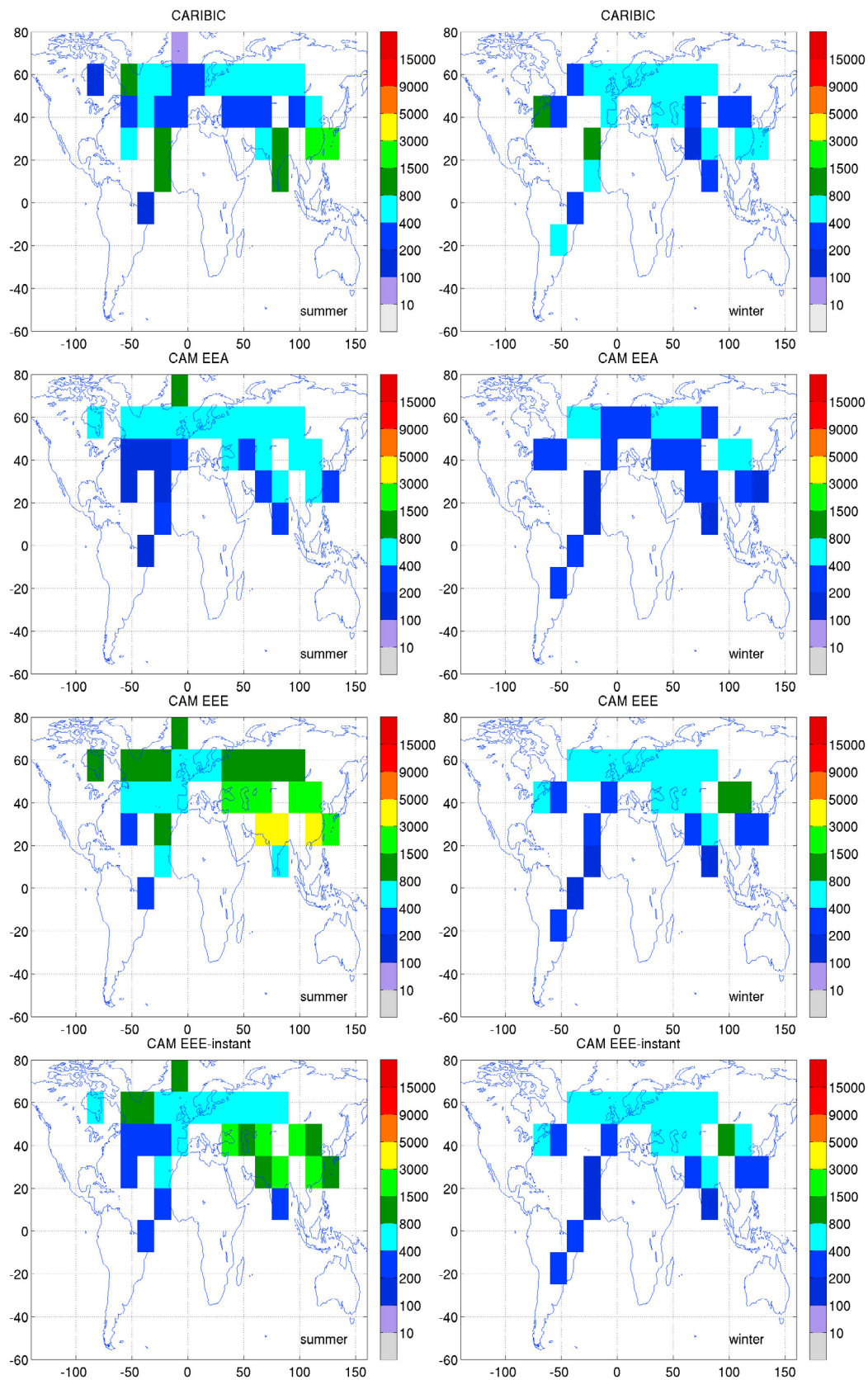


Figure 7. Northern hemisphere summer (May–September) and winter (November–March) N_{4-12} median concentration (particles cm^{-3} STP) for CARIBIC observations, the *EEA* simulation, the *EEE* simulation and the *EEE-instant* simulation. Note that the color scale is chosen for an easy comparison with *Heintzenberg et al.* [2011].

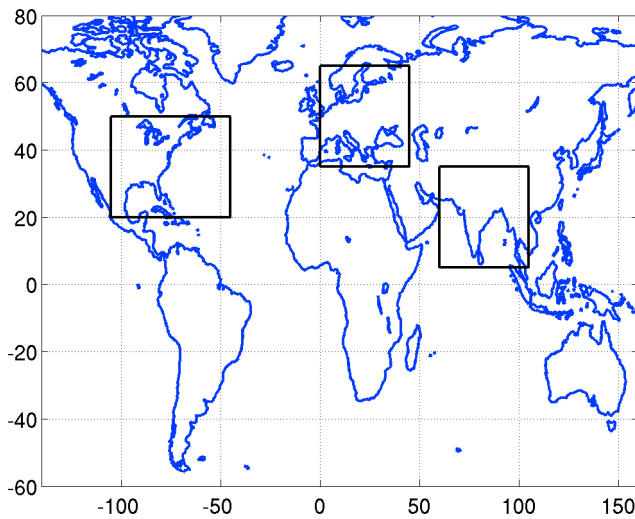


Figure 8. Selected study regions for annual variability plots: U.S., Europe and India.

3.2.2. Number Frequency Distributions and Vertical Profiles

[26] The simulated number frequency distributions for N_{12} in both the tropics (Figure 11) and at midlatitudes (Figure 12) agree fairly well with observations in terms of the shape of the distributions. However, similar to the N_{4-12} distributions, all modeled N_{12} distributions are narrower compared to the observations, especially in the tropics. This could, once again, indicate too little diffusive mixing in the model in the upper troposphere. A varying source strength is less likely to contribute to the discrepancy as the number of N_{12} particles in general is more sensitive to growth processes such as coagulation and condensation. There is also a tendency for underestimating the frequency in the high concentration range, especially in the *EEA* simulation. Table 2 shows that if the *CARIBIC* data is averaged over $2^\circ \times 2^\circ$, the agreement is better with the model simulations in terms of median and mean values.

[27] For the *CARIBIC* observations, the vertical profile of the N_{12} distribution versus potential temperature (Figure 6) is similar to the one for N_{4-12} , but with higher number concentrations and less variability. The model displays a vertical distribution of the median N_{12} that resembles the observed one. However, in the model, the concentrations are higher (median concentration overestimated by up to a factor of three) and the vertical gradient is steeper, pointing toward a too weak mixing in the upper troposphere in the model. All three model versions display a lower variability in N_{12} (10, 25, 75 and 90-percentiles) compared to observations.

3.2.3. Seasonal Variability

[28] A clear seasonal variation in the N_{12} number concentration is displayed in both the *CARIBIC* data and in the model simulations, with higher concentrations during the northern hemisphere summer (Figure 13). Both summer and winter concentrations are overestimated by the model and the difference between the seasons is also larger in the model.

[29] Figure 14 displays the annual variation in N_{12} for the different regions defined by Figure 8. For the U.S. region, the highest concentrations are measured by *CARIBIC* during June through September and the lowest during October

through December. This is similar to what was observed for the N_{4-12} concentration suggesting that a substantial part of the N_{12} aerosols are a direct result of new particle formation. The observed seasonal variability is fairly well captured by the model (model estimates are within the 25- and 75-percentiles of the observations) although the early winter concentrations tend to be overestimated. In the model, direct transport of carbonaceous particles appears to be a substantial source of the upper tropospheric N_{12} aerosol during the northern hemispheric summer months. There is a difference

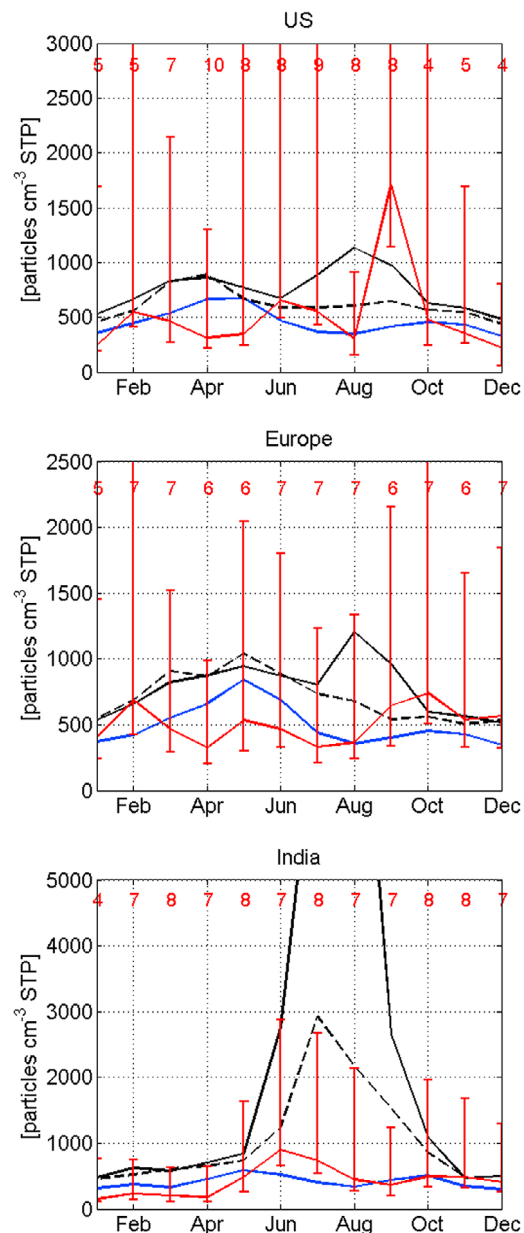


Figure 9. Annual cycle of measured (red) and modeled median N_{4-12} number concentration for the selected areas displayed in Figure 8. Blue color represents the *EEA* simulation, black solid the *EEE* simulation and black dashed the *EEE-instant* simulation. Error bars denote 25- and 75-percentiles. Red digits at the top of each plot indicate the number of $15^\circ \times 15^\circ$ grid cells of *CARIBIC* data available for evaluation.

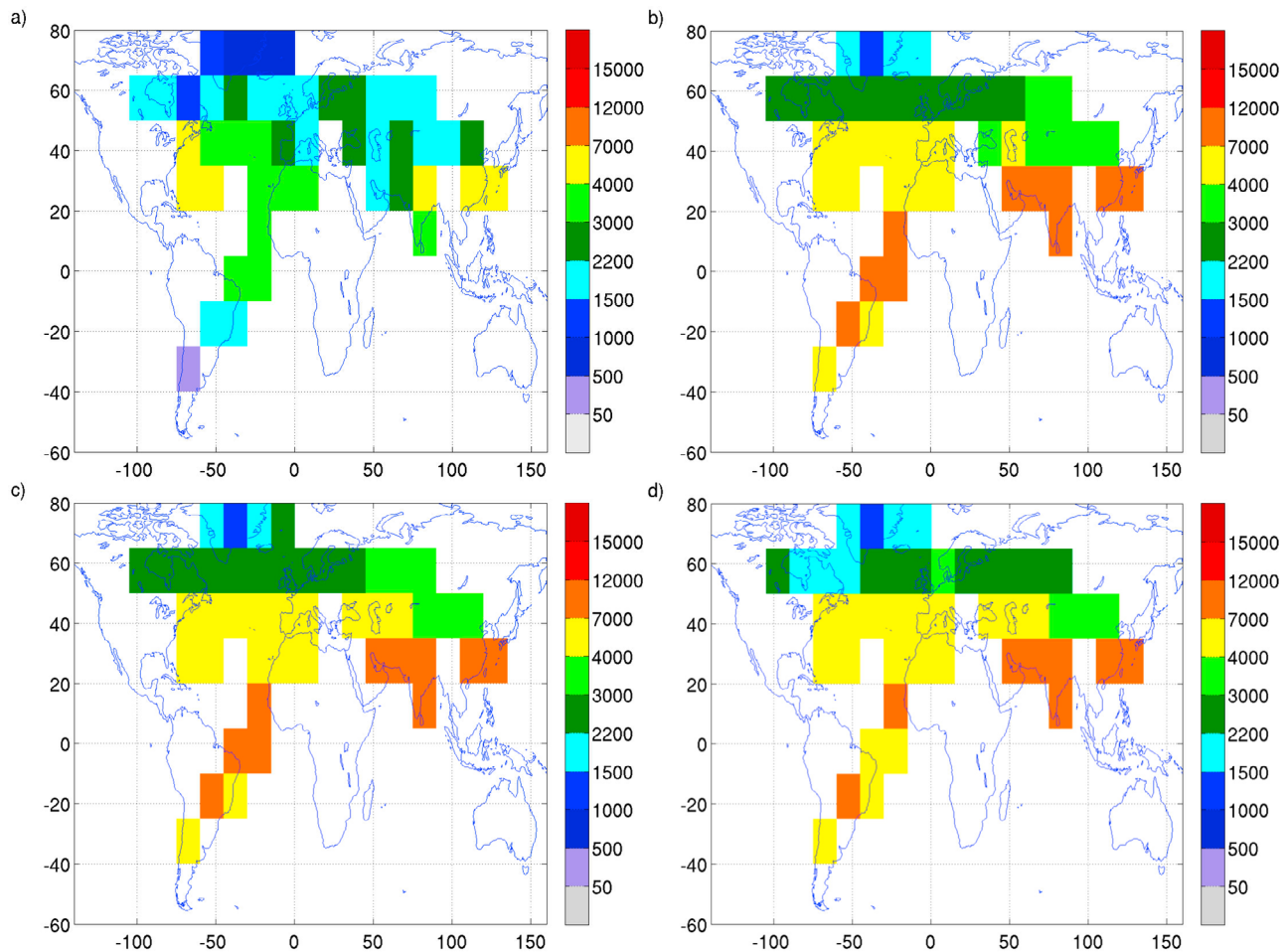


Figure 10. Annual median N_{12} number concentration (particles cm^{-3} STP) between 200 and 300 hPa for (a) CARIBIC observations, (b) *EEA* simulation, (c) *EEE* simulation and (d) *EEE-instant* simulation. Note that the color scale is chosen for an easy comparison with *Heintzenberg et al.* [2011].

of up to 70% between the model output (both from the *EEA* and the *EEE* simulations) if we include or exclude carbonaceous particles (gray lines in Figure 14). The model output excluding carbonaceous particles generally represents the double peak in the summer maximum seen in the observations better than the model output including carbonaceous aerosols. This may indicate a too strong direct transport of carbonaceous particles.

[30] On a global and annual average, the carbonaceous particles constitute approximately 20–30% of the modeled UT/LMS N_{12} particle number in the model. In the tropics, the UT/LMS number and mass concentration of pure BC and OC are 30–40% of the boundary layer (BL) concentration in both *EEE* and *EEA*. This number seems high considering that *Ekman et al.* [2006] estimated that approximately 10% of the BL concentration of BC can reach the top of a tropical deep convective cloud. In the model, to simplify the calculations, a prescribed supersaturation at cloud base of 0.1% for OC and 0.2% for sulfate and mixed aerosols is applied. This type of simplification appears to give rise to an unrealistic vertical transport of particles to the UT/LMS region.

[31] Over Europe and Asia, the CARIBIC observations reveal a clear seasonal cycle similar to the observed one for

the U.S. region. The highest N_{12} is measured in June (significant at 90% confidence level over Europe) and September/October and the lowest during the winter months. The model tends to overestimate the observed N_{12} , especially in summer and especially in the *EEE* simulation over India. Once again, the model fails to reproduce the double peak maximum during summer, which is visible in the CARIBIC data, although there is tendency to a double peak in the *EEE-instant* data excluding carbonaceous aerosols. This supports the hypothesis of a too strong vertical transport of carbonaceous aerosols in the model. In addition, the monthly averaging of the data in *EEE* and *EEA* appears to cause a substantial bias.

[32] The large vertical transport of carbonaceous N_{12} particles in the tropics is consistent with the underestimate of the N_{4-12} concentration in the same region as the high number concentrations of N_{12} particles efficiently depletes the available H_2SO_4 and increases the coagulation of newly formed particles.

4. Discussion and Conclusions

[33] In this study, we have compared observed large-scale distributions of nucleation mode (N_{4-12} , $4 \leq d \leq 12$ nm) and

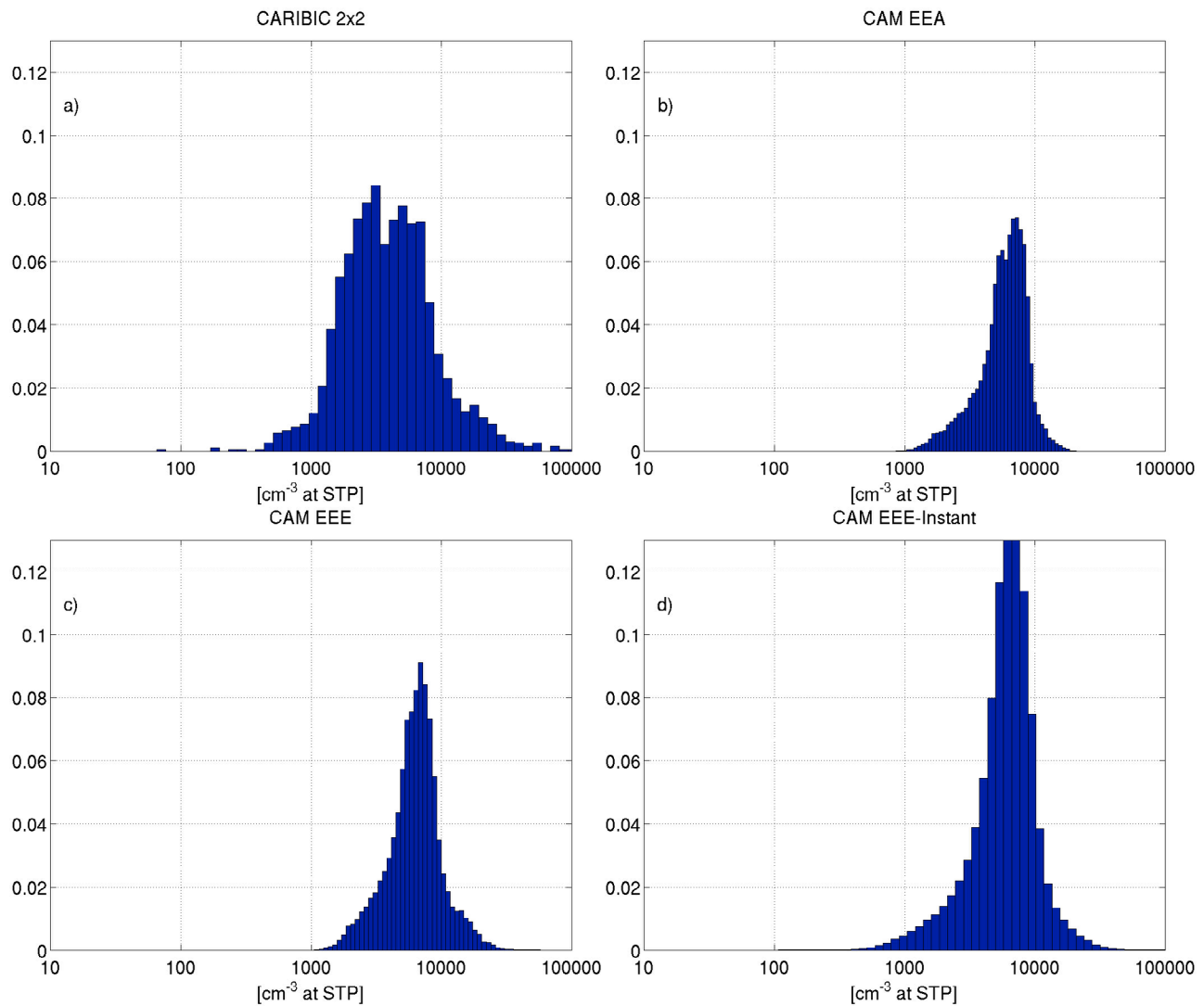


Figure 11. Frequency distribution for N_{12} particles in the tropics (25°S to 25°N) for all measurement/model data points in all the grid cells displayed in Figure 1.

Aitken mode (N_{12} , $d > 12$ nm) particle number concentrations in the upper troposphere and lowermost stratosphere (UT/LMS, altitude range, here 200–300 hPa) obtained from the CARIBIC project [Brenninkmeijer *et al.*, 1999, 2007] with global model simulations obtained using the MIT-CAM3 model [Kim *et al.*, 2008]. Three different model versions of the MIT-CAM3 were applied, one including aerosol chemical mixtures (*EEA*), and two excluding aerosol mixtures (*EEE* and *EEE-instant*). Monthly averaging of the model output is applied for the *EEA* and *EEE* simulations, whereas an instantaneous output every six hours is applied for the *EEE-instant* simulation.

[34] The model predicts global median UT/LMS concentrations in fair agreement (within a factor of two) with the observations indicating that the relatively simplified binary $\text{H}_2\text{SO}_4\text{-H}_2\text{O}$ nucleation parameterization applied in the model produces reasonable results in the UT/LMS. However, the N_{4-12} concentration is in general underestimated in the tropics (by up to 70%) as well as close to strong emission sources (of SO_2 and primary particles) whereas it is

overestimated (by up to several orders of magnitudes) at higher latitudes. N_{12} is overestimated in general (approximately by a factor of two) and in particular in the tropics and downwind emission sources. The modeled and observed N_{12} are in rather good agreement in terms of spatial (both vertical and horizontal) and temporal variability whereas the agreement for the N_{4-12} particles is poor.

[35] With the analysis conducted in the present study, it is not possible to pinpoint the main cause of the overestimate by the model of N_{4-12} particles at midlatitudes. However, the narrower frequency distribution in the model and the skew toward higher number concentrations indicates a too weak modeled mixing in the UT/LMS region. Sensitivity simulations targeted at different physical processes such as mixing, aerosol growth and scavenging are needed to give more firm conclusions. The underestimate of N_{4-12} in the tropics appears to be caused mainly by a too large vertical transport of carbonaceous particles that depletes the available H_2SO_4 and increases the coagulation of newly formed particles.

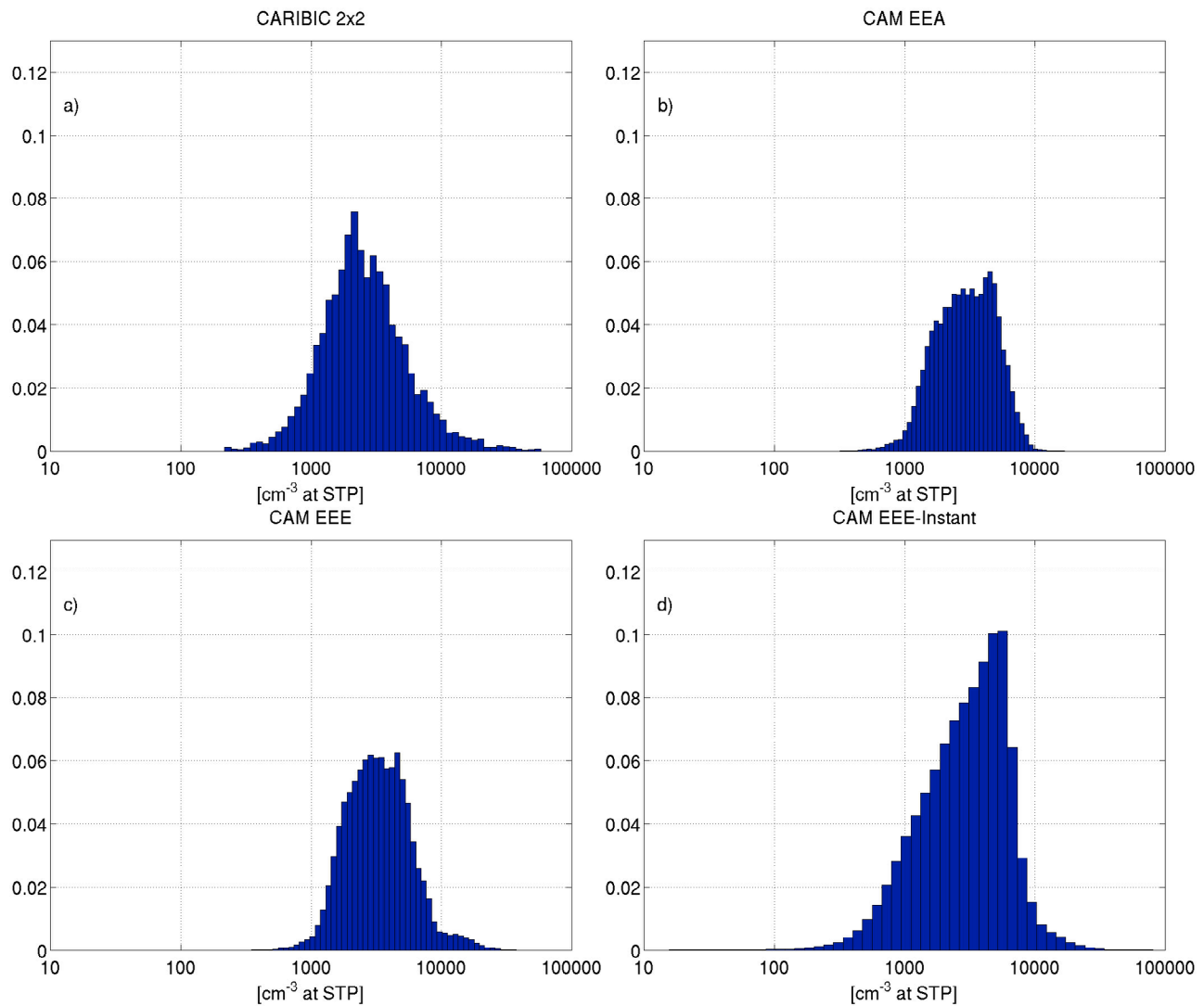


Figure 12. Frequency distribution for N_{12} particles at midlatitudes (35°S to 65°N) for all measurement/model data points in all the grid cells displayed in Figure 1.

[36] The signature in the temporal variability of the CARIBIC data with a double peak maximum observed over three regions in both N_{4-12} and N_{12} , suggests that a substantial part of the UT/LMS N_{12} population is a result of in situ new particle formation. For the N_{4-12} particles, the modeled seasonal variability is in poor agreement with CARIBIC data. This may, at least partly, be a result of the annually constant SO_2 emissions applied in the model. Another factor could be the lack of condensable organic compounds in the model that may help growth of newly formed clusters in the UT/LMS region [Ekman *et al.*, 2008; Kulmala *et al.*, 2006] or even the formation of the clusters [Kirkby *et al.*, 2011].

[37] Both the model and the observations display N_{12} concentrations that are higher in summer than in winter.

However, the model overestimates the difference between the summer and winter season. The overestimate of N_{12} particles is particularly pronounced during the summer months over Europe and India. This result also indicates a too large vertical transport of carbonaceous particles to the UT/LMS (as the convective transport should be stronger during summer compared to winter months). Our results corroborate those by Koch *et al.* [2009] who compared flight measurements of BC with global multimodel simulations. They found that the models generally overestimated BC concentrations in the free troposphere and suggested that the models may lack some upper-level removal process.

[38] A number of complications arise when comparing the CARIBIC data with the MIT-CAM model results. For example, the comparison between the *EEE* and *EEE-instant*

Figure 13. Northern hemisphere summer (May–September) and winter (November–March) N_{12} median concentration (particles cm^{-3} STP) for CARIBIC observations, the *EEA* simulation, the *EEE* simulation and the *EEE-instant* simulation. Note that the color scale is chosen for an easy comparison with Heintzenberg *et al.* [2011].

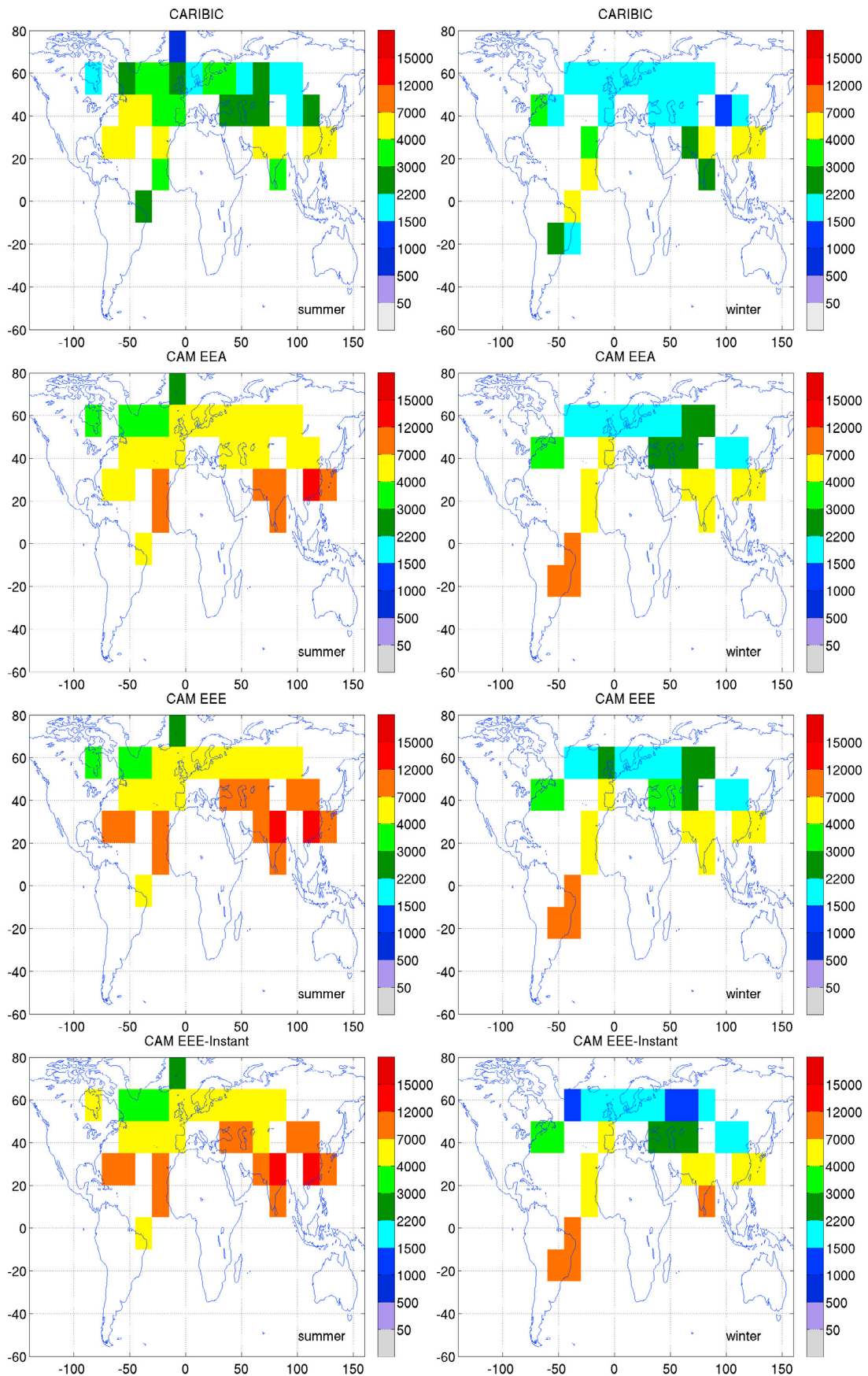


Figure 13

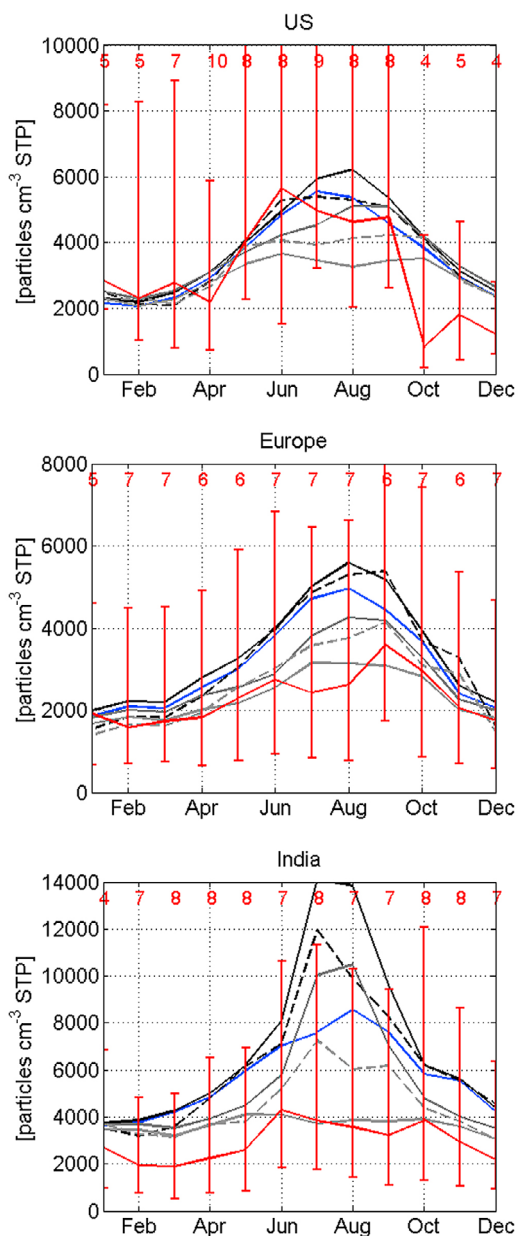


Figure 14. Annual cycle of measured (red) and modeled median N_{12} number concentration for the selected areas displayed in Figure 8. Blue color represents the *EEA* simulation, black solid the *EEE* simulation and black dashed the *EEE-instant* simulation. Error bars denote 25- and 75-percentiles. Also shown for comparison are modeled values for *EEE* (dark-gray line), *EEA* (light-gray line) and *EEE-instant* (light-gray dashed line) when neglecting all carbonaceous aerosols in the treatment of the output data. Red digits at the top of each plot indicate the number of $15^\circ \times 15^\circ$ grid cells of CARIBIC data available for evaluation.

simulation results shows that care has to be taken when choosing between instantaneous and averaged model output. The instantaneous output results in a more realistic variability range of the sub-micrometer aerosol concentrations and tropical tropopause temperatures, but gives at the same

time rise to bi-modal peaks in the frequency distribution which may be due to that the output frequency is too sparse (compared to the real diurnal cycle). Care must also be taken when choosing the measurement data to compare with, as several thousand flight kilometers of measurement data alone does not automatically imply that the data are representative for the time and region of interest (number of meteorological conditions, potential bias with respect to local time of day, etc.).

[39] This study is limited to a comparison between modeled and observed number concentrations of sub-micrometer aerosol particles. To strengthen the analysis, long-term and large-scale size-resolved particle mass and composition measurements would be beneficial (as they are currently carried out in CARIBIC) as well as measurements of aerosol precursor gases such as SO_2 and H_2SO_4 . Concurrent observations (or satellite retrievals) of cloud and precipitation processes would also be valuable [cf., e.g., Weigelt et al., 2009].

[40] **Acknowledgments.** A. Ekman would like to thank the Bert Bolin Centre for Climate Research and the Vinnova-VINNMER program for financial support. M. Hermann and the CARIBIC team are deeply grateful to the airlines LTU and Lufthansa for their strong support of CARIBIC. The development of the CARIBIC system was financially supported by the German Ministry of Education and Science (AFO 2000 program) and its operation benefited and benefits from the European Commission's DGXII Environment RTD 4th, 5th, 6th, and 7th Framework programs. P. Groß would like to thank the German Academic Exchange Service (DAAD) for the financial support of his stay in Stockholm. C. Wang thanks the U.S. NSF (ATM-0329759 and AGS-0944121) for supporting the development of MIT-NCAR aerosol-climate model.

References

- Adams, P. J., and J. Seinfeld (2002), Predicting global aerosol size distributions in general circulation models, *J. Geophys. Res.*, *107*(D19), 4370, doi:10.1029/2001JD001010.
- Albrecht, B. A. (1989), Aerosols, cloud microphysics, and fractional cloudiness, *Science*, *245*(4923), 1227–1230, doi:10.1126/science.245.4923.1227.
- Babiker, M., et al. (2001), The MIT Emissions Prediction and Policy Analysis (EPPA) Model: Revisions, sensitivities, and comparison of results, *Rep. 71*, 94 pp., Mass. Inst. of Technol., Cambridge, Mass. [Available at http://web.mit.edu/globalchange/www/MITJPSPGC_Rpt71.pdf].
- Barth, M. C., P. J. Rasch, J. T. Kiehl, C. M. Benkovitz, and S. E. Schwartz (2000), Sulfur chemistry in the National Center for Atmospheric Research Community Climate Model: Description, evaluation, features, and sensitivity to aqueous chemistry, *J. Geophys. Res.*, *105*, 1387–1415, doi:10.1029/1999JD900773.
- Bell, N., D. Koch, and D. T. Shindell (2005), Impacts of chemistry-aerosol coupling on tropospheric ozone and sulfate simulations in a general circulation model, *J. Geophys. Res.*, *110*, D14305, doi:10.1029/2004JD005538.
- Borrmann, S., S. Solomon, J. E. Dye, D. Baumgardner, K. K. Kelly, and K. R. Chan (1997), Heterogeneous reactions on stratospheric background aerosols, volcanic sulfuric acid droplets, and type I polar stratospheric clouds: Effects of temperature fluctuations and differences in particle phase, *J. Geophys. Res.*, *102*, 3639–3648, doi:10.1029/96JD02976.
- Borrmann, S., et al. (2010), Aerosols in the tropical and subtropical UT/LS: In-situ measurements of submicron particle abundance and volatility, *Atmos. Chem. Phys.*, *10*, 5573–5592, doi:10.5194/acp-10-5573-2010.
- Boville, B. A., P. J. Rasch, J. J. Hack, and J. R. McCaa (2006), Representation of clouds and precipitation processes in the Community Atmosphere Model Version 3 (CAM3), *J. Clim.*, *19*, 2184–2198, doi:10.1175/JCLI3749.1.
- Brenninkmeijer, C. A. M., et al. (1999), CARIBIC—Civil aircraft for global measurement of trace gases and aerosols in the tropopause region, *J. Atmos. Oceanic Technol.*, *16*, 1373–1383, doi:10.1175/1520-0426(1999)016<1373:CCAFGM>2.0.CO;2.
- Brenninkmeijer, C. A. M., et al. (2007), Civil aircraft for the regular investigation of the atmosphere based on an instrumented container: The new CARIBIC system, *Atmos. Chem. Phys.*, *7*, 4953–4976, doi:10.5194/acp-7-4953-2007.
- Brock, C. A., P. Hamill, J. C. Wilson, H. H. Jonsson, and K. R. Chan (1995), Particle formation in the upper tropical troposphere: A source of

- nuclei for the stratospheric aerosol, *Science*, 270, 1650–1653, doi:10.1126/science.270.5242.1650.
- Charlson, R., S. E. Schwartz, J. M. Hales, R. D. Cess, J. A. Coakley, J. E. Hansen, and D. J. Hofmann (1992), Climate forcing by anthropogenic aerosols, *Science*, 255, 423–430, doi:10.1126/science.255.5043.423.
- Clarke, A. D., and V. Kapustin (2002), A Pacific aerosol survey. Part I: A decade of data on particle production, transport, evolution, and mixing in the troposphere, *J. Atmos. Sci.*, 59, 363–382, doi:10.1175/1520-0469(2002)059<0363:APASPI>2.0.CO;2.
- Clement, C. F., I. J. Ford, C. H. Twohy, A. Weinheimer, and T. Campos (2002), Particle production in the outflow of a midlatitude storm, *J. Geophys. Res.*, 107(D21), 4559, doi:10.1029/2001JD001352.
- Clement, C. F., L. Pirjola, C. H. Twohy, I. J. Ford, and M. Kulmala (2006), Analytic and numerical calculations of the formation of a sulphuric acid aerosol in the upper troposphere, *J. Aerosol Sci.*, 37, 1717–1729, doi:10.1016/j.jaerosci.2006.06.007.
- Collins, W. D., et al. (2006), The Community Climate System Model Version 3 (CCSM3), *J. Clim.*, 19, 2122–2143, doi:10.1175/JCLI3761.1.
- de Reus, M., J. Ström, P. Hoor, J. Lelieveld, and C. Schiller (1999), Particle production in the lowermost stratosphere by convective lifting of the tropopause, *J. Geophys. Res.*, 104, 23,935–23,940, doi:10.1029/1999JD900774.
- Ekman, A. M. L., C. Wang, J. Ström, and R. Krejci (2006), Explicit simulation of aerosol physics in a cloud-resolving model: Aerosol transport and processing in the free troposphere, *J. Atmos. Sci.*, 63, 682–696, doi:10.1175/JAS3645.1.
- Ekman, A. M. L., R. Krejci, A. Engström, J. Ström, M. de Reus, J. William, and M. O. Andreae (2008), Do organics contribute to small particle formation in the Amazonian upper troposphere?, *Geophys. Res. Lett.*, 35, L17810, doi:10.1029/2008GL034970.
- English, J. M., O. B. Toon, M. J. Mills, and F. Yu (2011), Microphysical simulations of new particle formation in the upper troposphere and lower stratosphere, *Atmos. Chem. Phys.*, 11, 9303–9322, doi:10.5194/acp-11-9303-2011.
- Gislason, S. R., and P. Torssander (2006), Response of sulfate concentration and isotope composition in Icelandic rivers to the decline in global atmospheric SO₂ emissions into the North Atlantic region, *Environ. Sci. Technol.*, 40, 680–686, doi:10.1021/es051325o.
- Griffin, R. J., D. Dabdub, D. Cocker III, and J. H. Seinfeld (1999), Estimate of global atmospheric organic aerosol from oxidation of biogenic hydrocarbons, *Geophys. Res. Lett.*, 26(17), 2721–2724.
- Heintzenberg, J., and R. Charlson (2009), *Clouds in the Perturbed Climate System Their Relationship to Energy Balance, Atmospheric Dynamics, and Precipitation*, 576 pp., MIT Press, Cambridge, Mass.
- Heintzenberg, J., M. Hermann, A. Weigelt, A. Clarke, V. Kapustin, B. Anderson, K. Thornhill, P. van Velthoven, A. Zahn, and C. Brenninkmeijer (2011), Near-global aerosol mapping in the upper troposphere and lowermost stratosphere with data from the CARIBIC project, *Tellus, Ser. B*, 63, 875–890, doi:10.1111/j.1600-0889.2011.00578.x.
- Hendon, H. H., and K. Woodberry (1993), The diurnal cycle of tropical convection, *J. Geophys. Res.*, 98, 16,623–16,637, doi:10.1029/93JD00525.
- Hermann, M. (2000), Development and application of an aerosol measurement system for use on commercial aircraft, PhD thesis, Univ. Leipzig, Leipzig, Germany.
- Hermann, M., and A. Wiedensohler (2001), Counting efficiency of condensation particle counters at low-pressures with illustrative data from the upper troposphere, *J. Aerosol Sci.*, 32, 975–991, doi:10.1016/S0021-8502(01)00037-4.
- Hermann, M., F. Stratmann, M. Wilck, and A. Wiedensohler (2001), Sampling characteristics of an aircraft-borne aerosol inlet system, *J. Atmos. Oceanic Technol.*, 18, 7–19, doi:10.1175/1520-0426(2001)018<0007:SCOAAB>2.0.CO;2.
- Hermann, M., J. Heintzenberg, A. Wiedensohler, A. Zahn, G. Heinrich, and C. A. M. Brenninkmeijer (2003), Meridional distributions of aerosol particle number concentrations in the upper troposphere and lower stratosphere obtained by Civil Aircraft for Regular Investigation of the Atmosphere Based on an Instrument Container (CARIBIC) flights, *J. Geophys. Res.*, 108(D3), 4114, doi:10.1029/2001JD001077.
- Hermann, M., et al. (2008), Submicrometer aerosol particle distributions in the upper troposphere over the mid-latitude North Atlantic—Results from the third route of “CARIBIC,” *Tellus, Ser. B*, 60, 106–117, doi:10.1111/j.1600-0889.2007.00323.
- Hofmann, D. J., and S. Solomon (1989), Ozone destruction through heterogeneous chemistry following the eruption of El Chichon, *J. Geophys. Res.*, 94, 5029–5041, doi:10.1029/JD094iD04p05029.
- Kärcher, B. (2003), Simulating gas-aerosol-cirrus interactions: Process-oriented microphysical model and applications, *Atmos. Chem. Phys.*, 3, 1645–1664, doi:10.5194/acp-3-1645-2003.
- Kettle, A. J., et al. (1999), A global database of sea surface dimethylsulfide (DMS) measurements and a procedure to predict sea surface DMS as a function of latitude, longitude, and month, *Global Biogeochem. Cycles*, 13, 399–444, doi:10.1029/1999GB900004.
- Kim, D., C. Wang, A. M. L. Ekman, M. C. Barth, and P. J. Rasch (2008), Distribution and direct radiative forcing of carbonaceous and sulfate aerosols in an interactive size-resolving aerosol–climate model, *J. Geophys. Res.*, 113, D16309, doi:10.1029/2007JD009756.
- Kirkby, J., et al. (2011), Role of sulphuric acid, ammonia and galactic cosmic rays in atmospheric aerosol nucleation, *Nature*, 476, 429–433, doi:10.1038/nature10343.
- Koch, D., et al. (2009), Evaluation of black carbon estimations in global aerosol models, *Atmos. Chem. Phys.*, 9, 9001–9026, doi:10.5194/acp-9-9001-2009.
- Krämer, M., et al. (2009), Ice supersaturations and cirrus cloud crystal numbers, *Atmos. Chem. Phys.*, 9, 3505–3522, doi:10.5194/acp-9-3505-2009.
- Kulmala, M., A. Reissell, M. Sipilä, B. Bonn, T. M. Ruuskanen, K. E. J. Lehtinen, V.-M. Kerminen, and J. Ström (2006), Deep convective clouds as aerosol production engines: Role of insoluble organics, *J. Geophys. Res.*, 111, D17202, doi:10.1029/2005JD006963.
- Lee, S.-H., et al. (2003), Particle formation by ion nucleation in the upper troposphere and lower stratosphere, *Science*, 301, 1886–1889, doi:10.1126/science.1087236.
- Lee, S.-H., et al. (2004), New particle formation observed in the tropical/subtropical cirrus clouds, *J. Geophys. Res.*, 109, D20209, doi:10.1029/2004JD005033.
- Lohmann, U., and J. Feichter (2005), Global indirect aerosol effects: A review, *Atmos. Chem. Phys.*, 5, 715–737, doi:10.5194/acp-5-715-2005.
- Lu, Z., et al. (2010), Sulfur dioxide emissions in China and sulfur trends in East Asia since 2000, *Atmos. Chem. Phys.*, 10, 6311–6331, doi:10.5194/acp-10-6311-2010.
- Mayer, M. R., J. H. Hyman, and J. Reilly (2000), Emissions inventories and time trends for greenhouse gases and other pollutants, *Tech. Note 1*, 49 pp., Joint Program on the Sci. and Policy of Global Change, MIT, Cambridge, Mass.
- Ott, W. R. (1990), A physical explanation of the lognormality of pollutant concentrations, *J. Air Waste Manage.*, 40, 1378–1383.
- Peters, M. D., and S. M. Kreidenweis (2007), A single parameter representation of hygroscopic growth and cloud condensation nucleus activity, *Atmos. Chem. Phys.*, 7, 1961–1971, doi:10.5194/acp-7-1961-2007.
- Søvde, O. A., M. Gauss, I. S. A. Isaksen, G. Pitari, and C. Marizy (2007), Aircraft pollution—A futuristic view, *Atmos. Chem. Phys.*, 7, 3621–3632, doi:10.5194/acp-7-3621-2007.
- Ström, J., H. Fischer, J. Lelieveld, and F. Schröder (1999), In situ measurements of microphysical properties and trace gases in two cumulonimbus anvils over western Europe, *J. Geophys. Res.*, 104, 12,221–12,226, doi:10.1029/1999JD900188.
- Thompson, A. M., L. C. Sparling, Y. Kondo, B. E. Anderson, G. L. Gregory, and G. W. Sachse (1999), Perspectives on NO, NO_y, and fine aerosol sources and variability during SONEX, *Geophys. Res. Lett.*, 26(20), 3073–3076, doi:10.1029/1999GL900581.
- Twohy, C. H., et al. (2002), Deep convection as a source of new particles in the midlatitude upper troposphere, *J. Geophys. Res.*, 107(D21), 4560, doi:10.1029/2001JD000323.
- Twomey, S. (1977), Influence of pollution on shortwave albedo of clouds, *J. Atmos. Sci.*, 34, 1149–1152, doi:10.1175/1520-0469(1977)034<1149:TIOPOT>2.0.CO;2.
- Vehkamäki, H., M. Kulmala, I. Napari, K. E. J. Lehtinen, C. Timmreck, M. Noppel, and A. Laaksonen (2002), An improved parameterization for sulfuric acid–water nucleation rates for tropospheric and stratospheric conditions, *J. Geophys. Res.*, 107(D22), 4622, doi:10.1029/2002JD002184.
- Vestreng, V., G. Myhre, H. Fagerli, S. Reis, and L. Tarrason (2007), Twenty-five years of continuous sulphur dioxide emission reduction in Europe, *Atmos. Chem. Phys.*, 7, 3663–3681, doi:10.5194/acp-7-3663-2007.
- Wang, C. (2004), A modeling study on the climate impacts of black carbon aerosols, *J. Geophys. Res.*, 109, D03106, doi:10.1029/2003JD004084.
- Weigel, R., et al. (2011), In situ observations of new particle formation in the tropical upper troposphere: The role of clouds and the nucleation mechanism, *Atmos. Chem. Phys.*, 11, 9983–10,010, doi:10.5194/acp-11-9983-2011.
- Weigelt, A., M. Hermann, P. F. J. van Velthoven, C. A. M. Brenninkmeijer, G. Schlaf, A. Zahn, and A. Wiedensohler (2009), Influence of clouds on aerosol particle number concentrations in the upper troposphere, *J. Geophys. Res.*, 114, D01204, doi:10.1029/2008JD009805.
- Wilson, J. C., W. T. Lai, and S. D. Smith (1991), Measurements of condensation nuclei above the jet stream: Evidence for cross jet transport by

- waves and new particle formation at high altitudes, *J. Geophys. Res.*, *96*, 17,415–17,423, doi:10.1029/91JD01357.
- Wilson, J., C. Cuvelier, and F. Raes (2001), A modeling study of global mixed aerosol fields, *J. Geophys. Res.*, *106*, 34,081–34,108, doi:10.1029/2000JD000198.
- Zahn, A., and C. A. M. Brenninkmeijer (2003), New directions: A chemical tropopause defined, *Atmos. Environ.*, *37*, 439–440, doi:10.1016/S1352-2310(02)00901-9.
- Zahn, A., et al. (2000), Identification of extratropical two-way troposphere-stratosphere mixing based on CARIBIC measurements of O₃, CO and ultrafine particles, *J. Geophys. Res.*, *105*, 1527–1535, doi:10.1029/1999JD900759.